Available online at www.sciencedirect.com
ScienceDirect
Journal of the European Ceramic Society 30 (2010) 1427–1435
www.elsevier.com/locate/jeurceramsoc

Electrical properties of barium titanate stannate functionally graded materials

Smilja Marković [a], Čedomir Jovalekić [b], Ljiljana Veselinović [a], Slavko Mentus [c], Dragan Uskoković [a,*]

[a] *Institute of Technical Sciences of the Serbian Academy of Sciences and Arts, Knez Mihailova 35/IV, 11001 Belgrade, Serbia*
[b] *Institute for Multidisciplinary Research, Belgrade, Serbia*
[c] *Faculty of Physical Chemistry, University of Belgrade, St. Trg 12-16, Belgrade, Serbia*

Received 6 July 2009; received in revised form 12 October 2009; accepted 27 October 2009
Available online 27 November 2009

Abstract

Barium titanate stannate (BTS) functionally graded materials (FGMs) with different tin/titanium concentration gradient were prepared by the powder-stacking method and uniaxially pressing process, followed by sintering. Impedance spectroscopy (IS) was used to determine the electrical characteristics of FGMs and ingredient BTS ceramics, as well as to distinguish the grain-interior and grain boundary resistivity of the ceramics. Activation energies of FGMs and ingredients were calculated. It has been established that for BTS ceramics the activation energy deduced from grain-interior conductivity (0.73–0.75 eV) is defined by chemical composition, while activation energy for grain boundary conductivity (1.07–1.25 eV) is influenced by microstructural development (density and average grain size). Furthermore, for FGMs, activation energy for grain-interior conductivity kept the intrinsic properties (0.74–0.78 eV) and did not depend on tin/titanium concentration gradient, while activation energy (1.03–1.29 eV) for grain boundary was determined by the microstructural gradient. No point dissipation was observed by IS, accordingly, no insulator interfaces (cracks and/or delamination) between graded layers were detected.

Keywords: Functionally graded materials; Sintering; Grain boundaries; Electrical properties; $BaTiO_3$ and titanates

1. Introduction

Emerging technologies are demanding new materials with electrical (dielectric, ferroelectric, piezoelectric) and/or magnetic multifunctional properties, enhancing structural performances, such as mechanical and thermal expansion.[1] Functionally graded materials (FGMs) satisfy this requirement. Graded materials, by definition, have properties which vary as a function of position.[2–4] Continuous changes in the properties of FGMs such as: chemical composition, grain size, porosity, etc., result in the gradient of mentioned features (dielectric, ferroelectric, piezoelectric, magnetic properties, mechanical strength and thermal conductivity). In the late 1980s, the concept of FGMs was proposed in a research field of thermal barrier and stress relief materials.[2] During the last two decades, after the pioneer works on FGMs for structural applications, more uses have been worked out, mostly focused on electronic and functional applications. FGMs have been used for the fabrication of various technological components, such as electrical devices (piezoelectric ceramics, thermoelectric semiconductors, etc.),[5–8] electrochemical ones (for example solid oxide fuel cells – SOFC, or high-efficiency hybrid direct energy conversion systems – HYDECS),[9–11] as well as biomaterials.[12,13] Nowadays, FGMs are established as an attractive class of materials in which it is possible to create a gradient of properties that cannot be attained in any spatially homogeneous materials.

The concept of FGMs has been used to produce barium titanate stannate electronic devices.[14–16] Barium titanate stannate (BTS) ceramic is a binary solid solution system composed of ferroelectric barium titanate, $BaTiO_3$, and non-ferroelectric barium stannate, $BaSnO_3$.[17,18] Both of them are of perovskite structures with an ABO_3 formula. The B sites of the solid solution are occupied by either titanium or tin ions. Partial isovalent substitution of Ti^{4+} by Sn^{4+} leads to a shifting of the paraelectric–ferroelectric phase transition (Curie point, T_c) to lower temperatures, from 120 °C for $BaTiO_3$ to 5°C for $BaTi_{0.85}Sn_{0.15}O_3$[16,17]; simultaneously the phase transition becomes diffuse. Furthermore, BTS materials have high values

* Corresponding author. Tel.: +381 11 2636 994; fax: +381 11 2185 263.
E-mail address: dragan.uskokovic@itn.sanu.ac.rs (D. Uskoković).

0955-2219/$ – see front matter © 2009 Elsevier Ltd. All rights reserved.
doi:10.1016/j.jeurceramsoc.2009.10.020

of dielectric permittivity, which depends on the tin content.[16,17] However, a maximum of relative dielectric permittivity, $\varepsilon_{r,max}$, exists merely in a narrow (Curie) temperature intervals. For commercial application of electroceramics, it is necessary to broaden out the maximum in permittivity, so that high permittivity can be obtained over a range of temperatures.[19] This is usually done by double-doping.[19] Nowadays, Curie temperature intervals can be broadened by producing functionally graded materials. It is shown that BTS FGMs have a relatively high dielectric permittivity in a wide temperature range. Their electrical characteristics (dielectric permittivity, position of $\varepsilon_{r,max}$ at the temperature scale, and width of Curie temperature intervals) can be tailored by modifying tin/titanium concentration gradient.[16]

Thus, because of high dielectric permittivity in a wide temperature range and lead-free relaxor behavior, BTS FGMs have practical and/or potential application, as electroceramics in electronic industry (i.e. ceramic capacitors, bending actuators,[14,15] microwave phase shifters,[20] sensors,[21] etc.). These electroceramics contain electro-active intra-granular (bulk) and inter-granular (grain boundary) regions. Grain boundaries are the origin of the specific function of many electroceramics; in particular, grain boundaries play an important or even a key functional role.[22,23] Grain boundaries act as barriers for the cross transport of the charge carriers. Often, the barrier character of the grain boundary is especially pronounced in the low temperature regime. At high temperatures these resistive grain boundary barriers are reduced giving rise to substantially field-enhanced leakage currents through the components. That is the reason why detailed electrical studies, especially the ones concerning grain boundary barriers, are important for complete knowledge of barium titanate-based materials characteristics. Despite of emerging applications of BTS FGMs, not many studies have been presented in the literature regarding either the electrical properties of their grain boundaries, or the activation energies for ionic conductivity.

Impedance spectroscopy (IS) is an accurate, non-destructive technique for the characterization of bulk materials, and other unspecific phases such as secondary phases, porosity, cracks, etc. Moreover, IS is a powerful technique to distinguish the grain-interior and grain boundary resistance contributions of many oxide ceramics with ionic or mixed conduction. As a method sensitive to chemical composition and microstructure, IS can be suitable for characterization of FGMs. It can be used for the examination of the influence of concentration gradient on electrical characteristics, as well as on microstructural and/or macrostructural (delamination and/or cracks) defects in FGMs. Macrostructural (geometrical) defects especially may be a problem in FGMs fabricated by the powders processing.

In the present study, several functionally graded barium titanate stannate materials, with different graded composition, were fabricated by the powder-stacking method and uniaxially pressing process, followed by sintering. The influence of titanium/tin concentration gradient on electrical characteristics, as well as microstructural and/or macrostructural defects of FGMs was studied using IS. The grain-interior and grain boundary contributions in BTS FGMs were separated; activation energies were calculated for both of them, as well compared to those of BTS ingredients. To the best of our knowledge, this is the first IS investigation of BTS FGM focused on establishing the influence of concentration gradient on electrical properties, also, microstructural and macrostructural defects.

2. Experimental

2.1. BTS powders

The initial BTS powders ($BaTi_{1-x}Sn_xO_3$, with nominal composition $x = 0.025$, 0.05, 0.07, 0.10 and 0.15, noted as BTS2.5, BTS5, BTS7, BTS10 and BTS15, respectively) were prepared by a conventional solid state reaction. A description of the BTS synthesis can be found elsewhere.[16]

Particle size distribution (d_{50} and span) was measured by laser particle size analyzer (PSA). The used instrument was Mastersizer 2000 (Malvern Instruments Ltd., UK), which covers the particle size range of 0.02–2000 μm. For the PSA measurements, the powders were dispersed in 2-propanol with the aid of an ultrasonic bath (low-intensity ultrasound, at a frequency of 40 kHz and power of 50 W), for 3 min. The phase structure of the BTS powders sintered at 1420 °C for 2 h was determined at room temperature, using a powder X-ray diffractometer (Philips PW 1050, Cu $K\alpha_{1,2}$ radiation, at 40 kV and 20 mA). The diffraction measurements were done over scattering angle 2θ from 20° to 120° with a step of 0.02° and a counting time of 15 s. Rietveld analysis on the XRD patterns was carried out using the FullProf software package (version 2.10). JCPDS database was used for phase identification.[24] Theoretical density of BTS2.5, BTS5, BTS7, BTS10 and BTS15 powders, tin content, average

Table 1
Characteristics of used BTS powders.

	BTS2.5	BTS5	BTS7	BTS10	BTS15
Formulae	$BaTi_{0.975}Sn_{0.025}O_3$	$BaTi_{0.95}Sn_{0.05}O_3$	$BaTi_{0.93}Sn_{0.07}O_3$	$BaTi_{0.9}Sn_{0.10}O_3$	$BaTi_{0.85}Sn_{0.15}O_3$
Nominal Sn content (mol%)	2.5	5.0	7.0	10.0	15.0
Crystal structure	Tetragonal	Tetragonal	Tetragonal	Tetragonal	Cubic
Crystallite size (nm)	36.6	45.0	45.8	52.1	43.5
V (Å^3)	64.38(1)	64.44(1)	64.44(1)	64.46(1)	65.05(1)
Theoretical density (g/cm^3)	6.06	6.10	6.14	6.19	6.22
d_{50} (nm)	330	390	365	345	340
Span	1.530	1.600	1.520	1.090	0.940

crystallite size and volume of unit cell were calculated according to the Rietveld analysis on the XRD data. The main characteristics of BTS powders are given in Table 1.

2.2. FGMs

Before they were pressed into pellets the BTS powders had been crushed and triturated in agate mortar in 2-propanol in order to ensure particle size uniformity. Different FGMs were fabricated by the powder-stacking method. The BTS powders with different stoichiometry were stacked sequentially in die; they were uniaxially pressed into cylindrical compacts (∅ 4 mm and $h \approx 2$ mm) under a pressure of 300 MPa along the thickness direction of the graded layers. The samples were sintered in air up to 1420 °C, using a heating rate of 10 °C/min, whereas the duration of isothermal sintering was 2 h. For comparison of electrical characteristics of FGMs and their ingredients, the BTS were sintered in the same conditions as FGMs. The density of sintered ceramic samples was determined by a mercury porosimetry.

The impedance spectroscopy (IS) analysis was used to characterize all investigated FGMs and separate ingredient BTS components using an Gamry EIS300 Impedance Analyzer at frequencies of 1 Hz–100 kHz. Measurements were done in air during cooling from 320 to 25°C; an applied voltage was 100 mV. As electrodes, high conductivity silver paste was applied onto both sides of the samples, parallel to the layers. During measurement, sample was put in an adequate holder placed in muff oven. A Pt–Rh thermocouple located in a hot-sample holder was used for temperature monitoring.

The impedance data were fitted by software *Z*-View2 (version 2.6 demo). All of the impedance data collected between 320 and 25 °C were normalized by multiplying by the geometrical factor g [cm], which yielded the specific resistivity ρ [Ω cm]. The geometrical factor was estimated for every singe sample from its geometry (g is defined as A/d, where A is the sample area and d the thickness of the sample). The data were cut at low-frequency end (between 1 and 4 Hz) in order to avoid to fit sample response dominated by noise.

Fractured surfaces of the sintered BTS ceramics were coated with Au. The micrographs of the fractured surfaces were taken using a scanning electron microscope (SEM model JSM 5300, operating at 30 kV).

3. Results and discussion

In our previous publication, temperature dependent dielectric permittivity of FGMs taken at fixed frequency of 1 kHz have been presented.[16] The permittivity measurements at the fixed frequency of 1 kHz gives information significant to practical applications of barium titanate-based ceramic materials.[25] However, a great deal of additional information can be obtained by varying frequency. For instance, polycrystalline materials may show a variety of frequency-dependent effects associated with heterogeneities, such as grain boundaries or surface layers, as well as with intrinsic properties of the grains of the materials under consideration. In such cases, fixed-frequency measurements not only give restricted amount of information but, in addition, any interpretation of fixed-frequency data may be ambiguous.[25,26] Generally, *ac* impedance spectroscopy allows separation of grain-interior, grain boundary, and electrode process of the ceramics.[27]

In particular, a typical complex impedance diagram, in the so-called Nyquist presentation (the plot of imaginary, Z'', *versus* real impedance, Z', with the frequency f as an independent parameter) of a sintered, low-conducting material between blocking electrodes, consists of three parts (a bulk semicircle, a grain boundary semicircle, and an electrode arc), ending at the origin point of coordinate system at infinite frequency. For sintered barium titanate-based materials, the high-frequency semicircle of the impedance spectra is attributed to the grain-interior impedance, the middle one is attributed to the grain boundary response, whereby the low-frequency arc (<0.1 Hz) corresponds to the electrode response.[25,28–31] The grain-interior and grain boundary resistance may be read as the diameter of appropriate arcs.

So, as the fixed-frequency measurements are insufficient to determine electrical properties of grain boundaries in FGMs, above all resistivity which is an important characteristic of electronic ceramics since grain boundaries act as barriers for the cross transport of the charge carriers and consequently prevent leakage currents through electronic components, therefore, temperature dependent *ac* impedance measurements were performed with the aim firstly to distinguish bulk and grain boundary contribution of the resistivity, furthermore to determine the activation energies for bulk and grain boundary ionic conductivity, for different FGMs.

According to IS spectra of BTS FGMs and BTS ingredients, measured at room temperature, it is observed that the shape of Nyquist plots follows a line with a large slope, without point dissipation, indicating high-quality ceramics. This is especially important for FGMs, meaning no insulator interfaces (cracks and/or delamination) between graded layers were produced during powders processing and high-temperature sintering. Estimated direct current (*dc*) specific resistivities, ρ_{dc}, of the ingredients have the values of 10^9 Ω cm (Table 2). As it is known, the room temperature resistivity of barium titanate-based materials depends mainly on the microstructural development associated with grain growth.[25] Precisely, resistivity increases with an increase of density and decrease of average grain size.[32] In our case, since the values of ρ_{dc} increases with increase of density while average grain size simultaneously increase (Table 2) it can be supposed that density rather than average grain size is the dominant factor for specific resistivity of BTS ceramics. Besides, estimated values of ρ_{dc} for FGMs are similar to those of the ingredients (Table 2). Thus, high specific resistivity of the BTS FGMs at room temperature (indicating low leakage currents) in addition to previously determined high relative permittivity in a wide temperature intervals,[16] make this materials suitable for practical application as capacitors.

Furthermore, in order to separate grain and grain boundary contribution of the ceramics specific resistivity, the IS data collected above T_c (when grain boundary resistivity decreases by four orders of magnitude, from 10^{10} to 10^6 Ω) were analyzed.

Table 2
Electrical and microstructural characteristics of sintered ingredients and BTS FGMs.

Sample	ρ_{dc} (GΩ cm)	E_{gi} (eV)	E_{gb} (eV)	D_{50} (μm)	ρ (g/cm^3)
BTS2.5	5.00	0.73 ± 0.01	1.07 ± 0.03	21.1	5.85
BTS5	0.95	0.73 ± 0.01	1.12 ± 0.06	16.7	5.80
BTS7	0.80	0.74 ± 0.02	1.18 ± 0.01	15.8	5.75
BTS10	0.50	0.73 ± 0.01	1.25 ± 0.02	14.2	5.70
BTS15	0.35	0.75 ± 0.01	1.16 ± 0.02	11.8	5.50
2.5/15	1.23	0.78 ± 0.01	1.29 ± 0.02	–	5.60
2.5/5/7	1.26	0.74 ± 0.02	1.17 ± 0.02	–	5.65
2.5/5/7/10	0.67	0.76 ± 0.01	1.06 ± 0.01	–	5.60
15/5/7	0.44	0.77 ± 0.02	1.03 ± 0.04	–	5.55

Fig. 1 shows the impedance spectra of: (a) 2.5/15 FGM and (b) its ingredients (BTS2.5 and BTS15) at temperatures between 320 and 210°C. For clarity's sake, IS for chosen temperatures are shown in Fig. 1. The low-frequency arc was not found at <230 °C, which may be due to the effect of electrode relaxation process overlapping with the grain boundary relaxation process. However, with the increase of temperature (≥230 °C) impedance spectra for all the samples contained two semicircles (arcs). According to the literature, the high-frequency arc is ascribed to grain-interior resistance, ρ_{gi}, while the low-frequency arc is ascribed to grain boundary resistance, ρ_{gb}. From Fig. 1 it can be seen that the shape of Nyquist plots depends on temperature, with a clear increase of grain-interior as well as grain boundary resistivity with decreasing temperature.

The impedance spectra of all the investigated BTS FGMs and those of the ingredients are very similar, showing the same trend. To be more specific, at temperatures between 320 and 230 °C all the impedance spectra exhibit two semicircles; in addition, the resistivity of grain-interior and grain boundary increase with decreasing temperature.

At temperatures above T_c, the grain boundary in BTS is *ca.* 20–30 times more resistive than the grain-interior. The higher

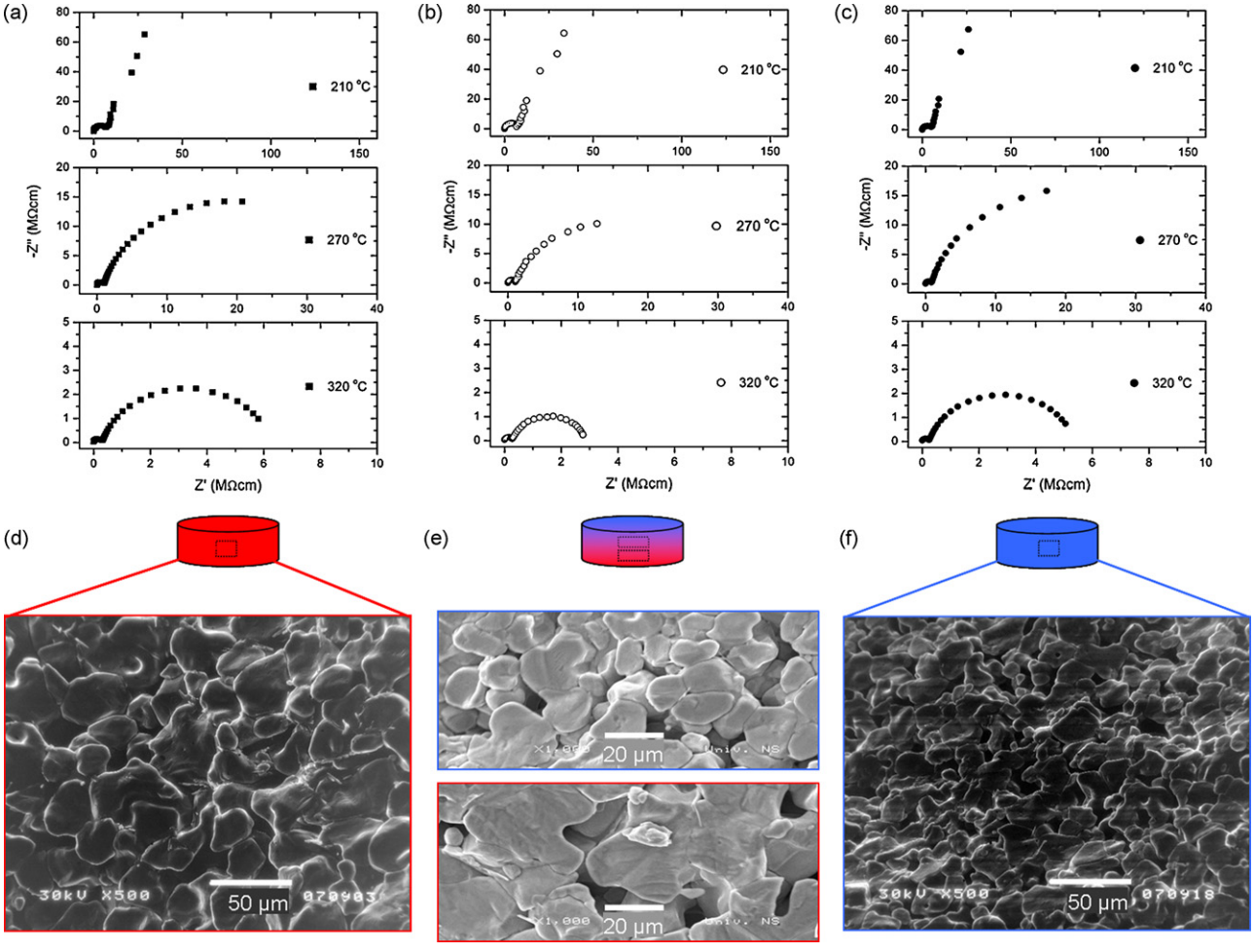

Fig. 1. IS spectra and microstructure of (a), (d) BTS2.5; (b), (e) 2.5/15 FGM; and (c), (f) BTS15, fired at 1420 °C.

grain boundary resistivity than that of grain-interior can be explained by following. Grain boundary resistance is influenced either by air gaps surrounding the grain-to-grain contacts or by high-impedance electrical inhomogeneity in the region of the necks between grains.[25] Grain boundaries are often laterally inhomogeneous, indicating that ideally conducting, and totally insulating interface regions are present. Precisely, solid grain boundary phases often only partially wet the grains, establishing a diminishing grain-to-grain contact; nano-pores along grain boundaries can also cause an imperfect contact between two grains. In such cases, insulating layer partly separates neighboring grains. Consequently, grain boundary resistance may be significantly higher than the ideal grain boundary resistance.[33] At temperature above T_c, the capacitance of air gaps increasingly dominates. The above-mentioned facts result in an apparent grain boundary semicircle, whose diameter is purely bulk-dependent.[33]

In the next stage, the recorded IS spectra were fitted by equivalent circuit in computer program Z-View2; as output values of ρ_{gi} and ρ_{gb} were obtained. In order to achieve this, it was necessary to find appropriate physics-based mathematical model for fitting. There is no *a priori* method to find the best equivalent circuit (mathematical model). For a given data set (i.e. impedance spectra) it is always possible to find more than one equivalent circuit model that can fit the data. Usually, in the case of polycrystalline materials, the complex impedance diagram in the form of two adjacent arcs, ascribed to grain-interior and grain boundary relaxation phenomena can be described by an equivalent circuit consisting of two parallel resistor (R) and capacitor (C) elements connected in series.[25,26,34] Here, the macroscopic impedance is just the sum of the individual RC impedances. The high-frequency arc corresponds to $R_{gi}C_{gi}$ response, whereas the low-frequency arc corresponds to $R_{gb}C_{gb}$ response. The impedance Z^* for that circuit can be described by Eq. (1)[25]:

$$Z^* = [R_b^{-1} + j\omega C_b]^{-1} + [R_{gb}^{-1} + j\omega C_{gb}]^{-1} \quad (1)$$

This mathematical model is valid for "ideal" systems, where the Nyquist plot is composed from semicircles with the centers on the x-axis. However, the observed plots of BTS FGMs, as well as the ingredients, at temperatures above the ferroelectric–paraelectric transition, were indeed the arcs of circles, but with the center on some distance below the x-axis. In order to fit these real system impedances, capacitor can be replaced with constant phase element (CPE) to account for non-Debye behavior (in fact, a capacitor is actually a CPE–one with a constant phase angle of 90°). When, instead of a C, a CPE is placed in parallel to a resistor, a depressed semicircle is produced. The existence of depressed semicircles in impedance spectra can be explained by a number of phenomena, depending on the nature of the investigated system. One of the physical explanations for CPE behavior is electrode (or surface) roughness; a rough or porous surface can cause a double-layer capacitance to appear as a constant phase element.[35] Another explanation is inhomogeneous reaction rates on a surface.[36] Both might be seen at polycrystalline surfaces[36] (it is our case too, considering that Ag electrodes were used). Another possible explanation for depressed semicircles of impedance spectra may be varying samples' thickness or composition.[37] The last undoubtedly matches with our case, where chemical composition varied throughout the thickness of FGM. One more reason for CPE behavior is non-uniform current distribution (it could be expected that the current density is fairly homogeneous near the center of the electrode, and normal to the surface; unfortunately, near the edge, the current density can be perturbed by "edge effects"; also, current flow may not be perfectly normal to the surface).[38,39]

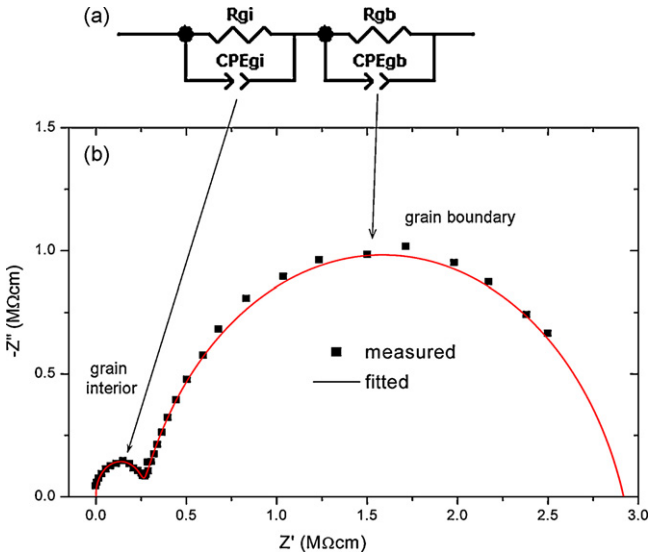

Fig. 2. (a) The model of equivalent circuit used for fitting of impedance spectra, and (b) an example of measured (on 2.5/15 FGM at 320 °C) and additionally fitted impedance spectrum..

Accordingly, to represent the impedance properties of BTS FGMs and BTS ingredients at temperatures above the ferroelectric–paraelectric transition, an equivalent circuit consisting of two parallel RCPE elements connected in series (Fig. 2(a)) was proved to be the best among possible equivalent circuits. An example of measured impedance data (full squares) additionally fitted (curve) with RCPE equivalent circuit is shown in Fig. 2(b). Good match between recorded and fitted data can be observed. After the fitting, the ρ_{gi} and ρ_{gb} were obtained as output from Z-View2 computer program. Furthermore, these values of specific resistivities [Ω cm] were converted to specific conductivities [S cm^{-1}] and used for the calculation of activation energies, separately for grain-interior and grain boundary conductivity. For microcrystalline, barium titanate-based materials, at higher temperatures, the total conductivity determined by IS can be ascribed to the mixed (ionic and electronic) conductivity. Also, it can be accentuated that at temperatures above T_c the electronic conductivity is significantly smaller than the ionic conductivity. Total ionic conductivity can be related to a migration energy or mobility barrier for oxygen vacancies.

The experimental data for total ionic conductivity were fitted as a function of temperature T following the Arrhenius law:

$$\sigma = \left(\frac{\sigma_o}{T}\right) \exp\left(-\frac{E_a}{k_B T}\right) \quad (2)$$

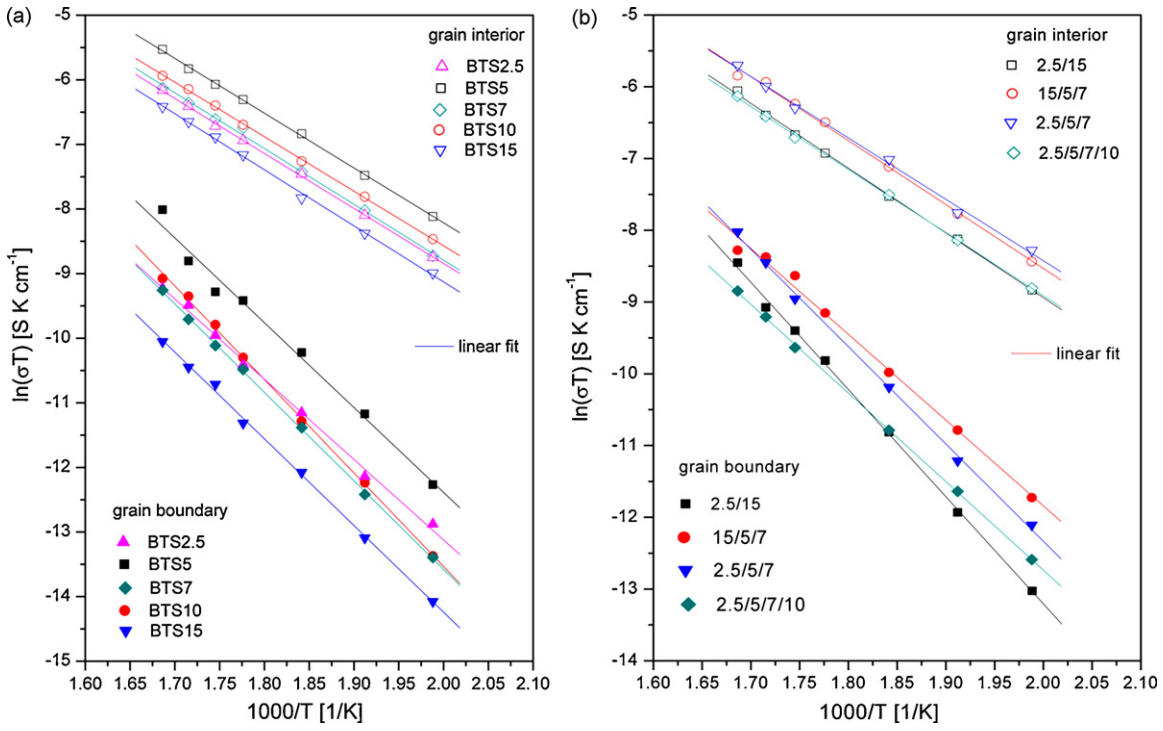

Fig. 3. Arrhenius plots of $\ln(\sigma T)$ *versus* $1000/T$ of: (a) BTS ceramics; and (b) different FGMs. Contributions of grain-interior and grain boundary are separated.

where E_a is the activation energy for ionic migration, k_B is the Boltzmann constant, and σ_o, the pre-exponential factor, is a constant related to the density of charge carriers. Total ionic conductivity can be separated on grain-interior ($\sigma_{gi} = 1/\rho_{gi}$) and grain boundary ($\sigma_{gb} = 1/\rho_{gb}$) contribution. Ionic conductivity in BTS occurs due to migration of O^{2-} ions through oxygen vacancies $V_O^{\bullet\bullet}$, which are produced due to slight loss of oxygen during sintering at 1420 °C according to the equation:

$$O_O \leftrightarrow 1/2O_2 + V_O^{\bullet\bullet} + 2e' \quad (3)$$

The oxygen loss at high temperatures (>*ca.* 1300 °C), Eq. (3), may be reversible during cooling in air or oxygen. The double-charged vacancies change to singly-charged oxygen vacancies below 580 °C[40]:

$$V_O^{\bullet\bullet} + e' \rightarrow V_O^{\bullet} \quad (4)$$

$V_O^{\bullet}$ is stable up to −269 °C, below which it becomes neutral. Therefore, during cooling after sintering, BTS materials that are electrically heterogeneous and consist of some frozen $V_O^{\bullet\bullet}$ as well as $V_O^{\bullet}$, were produced. All the species are written in accordance with Kröger-Vink notation of defects.[41]

Arrhenius plots of grain-interior and grain boundary conductivity, for BTS FGMs and BTS ingredients, are shown in Fig. 3. All obey the Arrhenius law and therefore activation energies (separately E_{gi} and E_{gb}) can be estimated from the slopes of these diagrams. Values of activation energies determined by least square fitting of specific conductivity data are listed in Table 2.

Here, due to the simplicity of the system, the electrical characteristics of BTS ingredients were presented first. The activation energy for grain-interior conductivity (E_{gi}) is determined by chemical composition. For BTS ingredients E_{gi} vary from 0.73 eV for BTS2.5 to 0.75 eV for BTS15, similar to those reported by Shvartsman et al.[42] and Wei and Yao.[18] In particular, small change of tin/titanium content in $BaTi_{1-x}Sn_xO_3$ (x from 0.025 to 0.15) negligibly influence intrinsic E_{gi} for $BaTiO_3$. This is in agreement with the XRD investigation, which shows that a small increase of Sn/Ti ratio does not significantly influence either lattice parameters, or the crystal structure (Table 1). This is a consequence of small differences in ionic radii of competitive Ti^{4+} [$R(Ti^{4+}) = 74.5$ pm] and Sn^{4+} [$R(Sn^{4+}) = 83.0$ pm].[43] Contrary, the activation energy for grain boundary conductivity, E_{gb}, is ruled by ceramics microstructure (density and average grain size, D_{50}), as well as by electrical inhomogeneity in the region of the necks between grains. As it is previously mentioned, density rather than average grain size is the dominant factor that influences the electrical characteristics of BTS ceramics. Here, E_{gb} vary from 1.07 to 1.25 eV for BTS2.5 to BTS10, respectively. That can be explained by following: an increase of tin content increases porosity and possibility for compositional inhomogeneity as well (which provokes electrical inhomogeneity); since pores (air gaps) and electrical inhomogeneities in ceramics act as barriers for oxygen ions migration E_{gb} increases, too. An exception to that behavior is observed for BTS15, which posses the highest porosity but not the highest activation energy. This fact can be explained by distinct characteristics of BTS15; its crystal structure is cubic, while the type of phase transition is diffuse.[16] All other BTS ingredients have tetragonal crystal structure and show λ-phase transition.

In the case of FGMs, E_{gi} vary in the range from 0.74 to 0.78 eV, similar to E_{gi} of ingredients. Thus, BTS FGMs

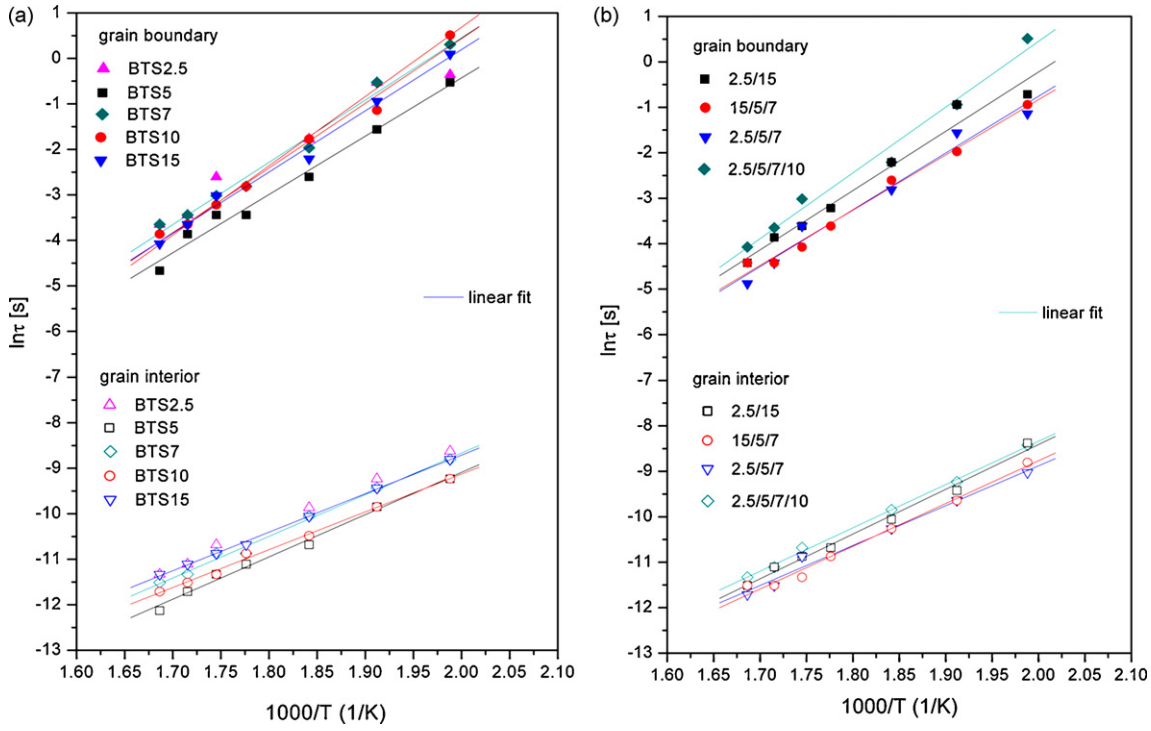

Fig. 4. Arrhenius plots of ln τ *versus* 1000/T of: (a) BTS ceramics; and (b) different FGMs. Contributions of grain-interior and grain boundary are separated.

keep intrinsic properties of BTS ingredient; what's more, E_{gi} does not depend on concentration gradient. Small discrepancy (±0.02 eV) between E_{gi} of ingredients and FGMs is probably caused by *IS* measurements error, provoked by spatially heterogeneous grain-interior in functionally graded materials. E_{gb} of different FGMs vary in the range of 1.03–1.29 eV. The highest E_{gb} of 1.29 eV, exhibits FGM 2.5/15, material that possesses the highest concentration/inhomogeneity and microstructural/porosity gradient. Air gaps on the contact between grains of different stoichiometry were produced due to different theoretical density of used powder, so high porosity gradient is produced in applied sintering conditions. As it is emphasized, these inhomogeneities and air gaps act as potential barriers for oxygen ions transport. Accordingly, FGM 15/5/7 with the smallest concentration (and inhomogeneity), microstructural and porosity gradient, has the smallest E_{gb} (1.03 eV). Therefore, E_{gb} is influenced by microstructural/porosity gradient, which are direct consequences of concentration gradient. Precisely, it is deduced that an increase of concentration gradient promotes the increase of potential inhomogeneity, microstructural and porosity gradients, as well as increase of E_{gb}.

The associated relaxation time, for grain-interior (τ_{gi}) and grain boundary (τ_{gb}), was also studied. Relaxation time is defined as $\tau = (2\pi f_{max})^{-1}$, where f_{max} is the frequency at the top of the Z'' *versus* Z' arcs.[28,44] The relaxation time is a geometry independent parameter; also it does not depend on microstructure. Instead,τ depends only on the intrinsic conductivity of material.[45] We found that for the studied BTS ingredients τ_{gi} is almost identical. The calculated values, for temperatures interval from 320 to 230 °C, fall in the range of 10^{-6} to 10^{-4} s, respectively. Besides, the calculated values for τ_{gb} are from 10^{-3} to 10^{0} s. In the case of FGMs the relaxation times, τ_{gi} as well as τ_{gb}, have values in the same range as for BTS ingredients; from 10^{-6} to 10^{-4} s for bulk relaxation process, and from 10^{-3} to 10^{0} s for grain boundary relaxation process. In Fig. 4 Arrhenius plots of ln τ *versus* 1000/T of BTS ingredients (Fig. 4(a)) and FGMs (Fig. 4(b)) are shown, separately for grain-interior (bottom) and grain boundary (top). Comparing the trends followed by the curves for BTS grain-interior (Fig. 4(a)) it can be concluded that there is only a small difference in the relaxation time distribution. This can be attributed to small differences in the chemical composition between BTS ingredients (from $BaTi_{0.975}Sn_{0.025}O_3$ to $BaTi_{0.85}Sn_{0.15}O_3$). These results are in accordance with E_{gi} calculated from conductivity data, which shows neglected differences between intrinsic properties of BTS (from 0.73 eV for $BaTi_{0.975}Sn_{0.025}O_3$ to 0.75 eV for $BaTi_{0.85}Sn_{0.15}O_3$). The same observation is valid for FGMs grain-interior (Fig. 4(b)). Obviously, grain boundary relaxation times are about three orders of magnitude larger than those of the grain-interior. Naturally, in the grain boundary structure the time spent in the relaxation process is longer. So, it can be emphasized that there is no significant difference between bulk neither grain-interior relaxation processes in BTS ingredients and BTS FGMs.

4. Conclusions

Barium titanate stannate functionally graded materials (BTS FGMs) with different tin/titanium concentration gradient were prepared by the powder-stacking method and uniaxially pressing process, followed by sintering. A variety of concentration

gradients were attained using BTS powders with different stoichiometry (from $BaTi_{0.975}Sn_{0.025}O_3$ to $BaTi_{0.85}Sn_{0.15}O_3$) stacked in different number of layers (from 2 to 4). A series of impedance spectra as a function of temperature were analyzed with the aim to define influence of titanium/tin concentration gradient on electrical characteristics of FGMs. No point dissipation is observed by *IS* and, accordingly, no insulator interfaces (cracks or delamination) between graded layers in FGMs are detected. Thus, uniaxially pressing of stacked powders, followed by sintering at 1420 °C has been proven to be an useful method for the preparation of high-quality BTS FGMs.

At room temperature, the specific resistivity of the BTS FGMs is very high ($10^9\ \Omega$ cm) indicating low leakage currents, consequently making these materials appropriate as capacitors.

The activation energy for grain boundary ionic conductivity is typically higher than that for the grain-interior transport, for both BTS ingredients and BTS FGMs.

The activation energy estimated from grain-interior conductivity depends on chemical composition. For ingredients and FGMs, the activation energy for grain-interior conductivity is very similar, varying in the range from 0.73 to 0.78 eV. Hence, it can be conclude that concentration gradient does not influence intrinsic conductivity.

Quite contrary, activation energy for grain boundary conductivity is different for FGMs and their ingredients. For BTS ingredients with tetragonal crystal structure and a ferroelectric phase transition of λ-type, E_{gb} increases from 1.07 to 1.25 eV, due to an increase of porosity and probably electrical inhomogeneity in the region of the necks between grains. An exception to this behavior was noticed for BTS15 with cubic crystal structure and a ferroelectric phase transition of diffuse type. For FGMs, the activation energy for grain boundary conductivity increases from 1.03 to 1.29 eV, influenced with the increase of concentration gradient. Precisely, an increase of concentration gradient promotes the increase of electrical inhomogeneity, microstructural and porosity gradients, i.e. the number of air gaps and inhomogeneities on the contacts between grains with different stoichiometry/microstructure increases promoting an increase of E_{gb}. FGM with the highest concentration gradient (2.5/15) posses the highest porosity gradient; consequently, this FGM shows the highest activation energy (1.29 eV) for grain boundary conductivity. Quite contrary, FGM with the smallest concentration gradient (15/5/7) posses the smallest porosity gradient, consequently, this FGM shows the smallest activation energy (1.03 eV) for grain boundary conductivity.

Relaxation processes in BTS ingredients and BTS FGMs are almost identical. In addition, grain boundary relaxation times are about three orders of magnitude larger than those of the grain-interior.

Acknowledgement

The Ministry of Science and Technological Development of the Republic of Serbia provided financial support under Grant No. 142006.

References

1. Sánchez-Herencia AJ, Moreno R, Jurado JR. Electrical transport properties in zirconia/alumina functionally graded materials. *J Eur Ceram Soc* 2000;**20**:1611–20.
2. Koizumi M. FGM activities in Japan. *Composites B* 1997;**28**:1–4.
3. Koizumi M, Niino M. Overview of FGM research in Japan. *MRS Bull* 1995;**20**:19–21 (Special Issue, Functionally Gradient Materials, ed. E. L. Fleitscher).
4. Kieback B, Neubrand A, Reidel H. Processing techniques for functionally graded materials. *Mater Sci Eng A* 2003;**362**:81–106.
5. Wu CC, Khan M, Moy W. Piezoelectric ceramics with functional gradient: a new application in material design. *J Am Ceram Soc* 1996;**79**:809–12.
6. Almajid AA, Taya M. 2D-elasticity analysis of FGM piezo-laminates under cylindrical bending. *J Intell Mater Syst Struct* 2001;**12**:341–51.
7. Joshi S, Mukherjee A, Schmauder S. Numerical characterization of functionally graded active materials under electrical and thermal fields. *Smart Mater Struct* 2003;**12**:571–9.
8. Dashevsky Z, Shusterman S, Dariel MP, Drabkin I. Thermoelectric efficiency in graded indium-doped PbTe crystals. *J Appl Phys* 2002;**92**:1425–30.
9. Liu Z, Han M-F, Miao W-T. Preparation and characterization of graded cathode $La_{0.6}Sr_{0.4}Co_{0.2}Fe_{0.8}O_{3-\delta}$. *J Power Sources* 2007;**173**:837–41.
10. Eguchi K, Hoshino T, Fujihara T. Performance analysis of FGM-based direct energy conversion system for space power applications. In: Ilschner B, Cherradi N, editors. *Third International Symposium on Structural Functional Gradient Materials Proceedings of FGM'94*. Lausanne, Switzerland: Presses Polytech. Univ. Romandes; 1995. p. 619–25.
11. Niino M, Koizumi M. Projected research on high-efficiency energy conversion materials. In: Ilschner B, Cherradi N, editors. *Third International Symposium on Structural and Functional Gradient Materials Proceedings of FGM'94*. Lausanne, Switzerland: Presses Polytech. Univ. Romandes; 1995. p. 601–5.
12. Thomas V, Zhang X, Catledge SA, Vohra YK. Functionally graded electrospun scaffolds with tunable mechanical properties for vascular tissue regeneration. *Biomed Mater* 2007;**2**:224–32.
13. Manjubala I, Sampath Kumar TS. Effect of TiO_2–Ag_2O additives on the formation of calcium phosphate based functionally graded bioceramics. *Biomaterials* 2000;**21**:1995–2002.
14. Steinhausen R, Kouvatov A, Beige H, Langhammer HT, Abicht H-P. Poling and bending behavior of piezoelectric multilayers based on $Ba(Ti,Sn)O_3$ ceramics. *J Eur Ceram Soc* 2004;**24**:1677–80.
15. Pientschke C, Kouvatov A, Steinhausen R, Seifert W, Beige H. Polarisation kinetics of electrically connected electroconductive ferroelectric multilayer structures. *J Eur Ceram Soc* 2005;**25**:2547–51.
16. Marković S, Mitrić M, Cvjetićanin N, Uskoković D. Preparation and properties of $BaTi_{1-x}Sn_xO_3$ multilayered ceramics. *J Eur Ceram Soc* 2007;**27**:505–9.
17. Smolenskii, G. A., Bokov, V. A., Isupov, N. N., Krainik, V. A., Pasynkov, R. E. and Shur, M. S., Ferroelectrics and anti-ferroelectrics (Izd. "Nauka" Leningradskii Otdeleniye, Leningrad 1971), 355–369 [in Russian].
18. Wei X, Yao X. Preparation, structure and dielectric property of barium stannate titanate ceramics. *Mater Sci Eng B* 2007;**137**:184–8.
19. West AR, Adams TB, Morrison FD, Sinclair DC. Novel high capacitance materials: $BaTiO_3$:La and $CaCu_3Ti_4O_{12}$. *J Eur Ceram Soc* 2004;**24**:1439–48.
20. Xiaoyong W, Yujun F, Xi Y. Dielectric relaxation behavior in barium stannate titanate ferroelectric ceramics with diffused phase transition. *Appl Phys Lett* 2003;**83**:2031–3.
21. Müller E, Drašar Č, Schilz J, Kaysser WA. Functionally graded materials for sensor and energy applications. *Mater Sci Eng A* 2003;**362**:17–39.
22. Rout SK, Panigrahi S, Bera J. Study of electrical properties of Ni-doped $SrTiO_3$ ceramics using impedance spectroscopy. *Bull Mater Sci* 2005;**28**:275–9.
23. Greuter F, Blatter G. Electrical properties of grain boundaries in polycrystalline compound semiconductors. *Semicond Sci Technol* 1990;**5**:111–37.
24. *JCPDS Database on CD-ROM*. Newton Square, PA: International Centre for Diffraction Data; 1999.

25. Hirose N, West AR. Impedance spectroscopy of undoped $BaTiO_3$ ceramics. *J Am Ceram Soc* 1996;**79**:1633–41.
26. Sinclair DC, West AR. Impedance and modulus spectroscopy of semiconducting $BaTiO_3$ showing positive temperature coefficient of resistance. *J Appl Phys* 1989;**66**:3850–6.
27. Bauerle JE. Study of solid electrolyte polarization by a complex admittance method. *J Phys Chem Solids* 1969;**30**:2657–70.
28. Macdonald JR, editor. *Impedance Spectroscopy*. New York/Chichester/Brisbane/Toronto/Singapore: John Wiley & Sons; 1987.
29. Morrison FD, Sinclair DC, West AR. Characterization of lanthanum-doped barium titanate ceramics using impedance spectroscopy. *J Am Ceram Soc* 2001;**84**:531–8.
30. V'yunov OI, Kovalenko LL, Belous AG, Belyakov VN. Oxidation of reduced Y-doped semiconducting barium titanate ceramics. *Inorg Mater* 2005;**41**:93–100.
31. Belous A, V'yunov O, Kovalenko L, Makovec D. Redox processes in highly yttrium-doped barium titanate. *J Solid State Chem* 2005;**178**:1367–75.
32. Tang CQ, Yao S. The defects, grain size and electrical property in the non-stoichiometric $BaTiO_3$ ceramics. *Cryst Res Technol* 2000;**35**:609–14.
33. Fleig J. The influence of non-ideal microstructures on the analysis of grain boundary impedances. *Solid State Ionics* 2000;**131**:117–27.
34. West AR, Sinclair DC, Hirose N. Characterization of electrical materials, especially ferroelectrics, by impedance spectroscopy. *J Electroceram* 1997;**1**:65–71.
35. Mulder WH, Sluyters JH, Pajkossy T, Nyikos I. Tafel current at fractal electrodes. Connection with admittance spectra. *J Electroanal Chem* 1990;**285**:103–15.
36. Kim C-H, Pyun S-I, Kim J-H. An investigation of the capacitance dispersion on the fractal carbon electrode with edge and basal orientations. *Electrochim Acta* 2003;**48**:3455–63.
37. Schiller CA, Strunz W. The evaluation of experimental dielectric data of barrier coatings by means of different models. *Electrochim Acta* 2001;**46**:3619–25.
38. Jorcin J-B, Orazem ME, Pebere N, Tribollet B. CPE analysis by local impedance analysis. *Electrochim Acta* 2006;**51**:1473–9.
39. Oldham KB. The RC time 'constant' at a disk electrode. *Electrochem Commun* 2004;**6**:210–4.
40. Moos R, Menesklou W, Härdtl KH. Hall mobility of undoped n-type conducting strontium titanate single crystals between 19 K and 1373 K. *Appl Phys A* 1995;**61**:389–95.
41. Kröger FA, Vink HJ. In: Seitz F, Turnball D, editors. *Solid State Physics: Advances in Research and Applications*, vol. 3. New York: Academic Press; 1956. p. 307–435.
42. Shvartsman VV, Kleemann W, Dec J, Xu ZK, Lu SG. Diffuse phase transition in $BaTi_{1-x}Sn_xO_3$ ceramics: an intermediate state between ferroelectric and relaxor behavior. *J Appl Phys* 2006;**99**:1241111–8.
43. Shannon RD, Prewitt CT. Effective ionic radii in oxides and fluorides. *Acta Crystallogr B* 1969;**25**:925–46.
44. Bucio L, Orozco E, Huanosta-Tera A. Relaxation and conductivity behaviour in the compounds: $FeRGe_2O_7$ (R = Pr, Tb). *J Phys Chem Solids* 2006;**67**:651–8.
45. Sooksaen P, Reaney IM, Sinclair DC. Crystallization and dielectric properties of borate-based ferroelectric $PbTiO_3$ glass-ceramics. *J Electroceram* 2007;**19**:221–8.